J. Mater. Environ. Sci. 7 (7) (2016) 2482-2497
ISSN : 2028-2508
CODEN: JMESCN

Anti-corrosive properties of benzothiazine derivatives on mild steel corrosion in 1 M HCl solution: Experimental and theoretical studies

M. Ellouz[1], H. Elmsellem[2*], N. K. Sebbar[1], H. Steli[5], K. Al Mamari[1,4], A. Nadeem[1], Y. Ouzidan[3], E. M. Essassi[1], I. Abdel-Rahaman[6], P. Hristov[7]

[1]*Laboratoire de Chimie Organique Hétérocyclique, URAC 21, Pôle de Compétences Pharmacochimie, Mohammed V University in Rabat, Faculté des Sciences, Av. Ibn Battouta, BP 1014 Rabat, Morocco.*
[2] *Laboratoire de chimie analytique appliquée, matériaux et environnement (LC2AME), Faculté des Sciences, B.P. 717, 60000 Oujda, Morocco*
[3]*Laboratoire de Chimie Organique Appliquee, Université Sidi Mohamed Ben Abdallah, Faculté des Sciences et Techniques, Route d'Immouzzer, BP 2202 Fes, Morocco.*
[4]*Department of Chemistry - Faculty of Education University of Hodiedah – Yemen.*
[5]*Laboratoire mécanique & énergétique, Faculté des Sciences, Université Mohammed Premier, Oujda, Maroc*
[6]*Department of Chemistry, College of Sciences, University of Sharjah, Sharjah, PO Box: 27272, UAE.*
[7]*Biodiversity Department, Institute of Biodiversity and Ecosystem Research – BAS, Sofia 1113, Bulgaria*

Received 09 Mar 2016, Revised 19 May 2016, Accepted 22 May 2016

**Corresponding author. E-mail : h.elmsellem@yahoo.fr; Tel : +212670923431*

Abstract

The corrosion inhibitory effect of two benzothiazine derivatives, namely methyl 2-(3-oxo-2,3-dihydro[1,4]benzothiazin-4-yl) acetate (P1) and (Z)-methyl 2-(2-benzylidene-3-oxo-2,3-dihydro[1,4] benzothiazin-4-yl) acetate (P2), on mild steel in 1M HCl has been studied using electrochemical impedance spectroscopy (EIS), Tafel polarization curves and weight loss measurements. It was found that the inhibition efficiency of the two investigated inhibitors increases with increase in concentration of inhibitors. P1 and P2 show corrosion inhibition efficiency of 93 and 96%, respectively at 10^{-3}M and 308 K. Impedance experimental data revealed a frequency distribution of the capacitance, simulated as constant phase element. Potentiostatic polarization study showed that P1 and P2 are mixed-type inhibitors in 1M HCl. The results obtained from electrochemical and weight loss studies were in reasonable agreement. The adsorption of P1 and P2 on steel surface obeys Langmuir's adsorption isotherm. The correlation between inhibition efficiency and molecular structure of the inhibitors is investigated by determination of chemical indexes, which were performed using density functional theory (DFT) at (B3LYP/6-31G) (d, p) level.

Keywords: Benzothiazine, Mild steel, Polarization, Electrochemical impedance spectroscopy, Quantum chemical calculations (DFT).

1. Introduction

In recent days, studies on steel corrosion phenomena have become an industrial and academic topic, especially in acid media [1,2]. This is because of the increasing industrial applications of acid solutions. The most important fields of applications are acid pickling, industrial cleaning, acid descaling, oil-well acidizing in oil recovery and the petrochemical processes. Aqueous solutions of acids are among the most corrosive media. So, the rate of corrosion at which metals are destroyed in acidic media is very high, especially when soluble corrosion products are formed. Therefore, investigating and exploring corrosion inhibitors for steel corrosion in acid solutions are not only important from an academic point of view but also for its practical applications[3-5].

It is well documented that 1,4-benzothiazin-3-one derivatives possess important pharmacological properties and play vital role in neurodegenerative diseases, such as Parkinson's disease and Alzheimer disease[6], vasodilators[7], anticataract agents[8], matrix metalloproteinase inhibitors[9]. According to the numerous examples, benzo[1,4]thiazin-3-one fragment can be considered as a typical "privileged" substructure[10].

The present investigation is concerned with the mechanism and efficiency of 3-oxo-[1,4]-benzothiazine derivatives (**P1** and **P2**) as corrosion inhibitor of mild steel in 1M HCl solution (**Scheme 1**).

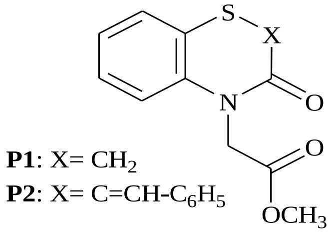

Scheme 1: Methyl 2-(2-substituted-[1,4]-benzothiazin-3-one-4-yl) acetate **(P1 and P2)** [11-12].

2. Experimental details

2.1. Synthesis of inhibitors

To a solution of [1,4]-benzothiazin-3-one derivative (**Pa** and **Pb**: 2 mmol), potassium carbonate (0.55 g, 4 mmol) and tetra *n*-butyl ammonium bromide (TBAB) (0.064 g, 0.2 mmol) in DMF (15 ml) was added methyl chloroacétate (0.35 ml, 4 mmol). Stirring was continued at room temperature for 12 hrs. The mixture was filtered and the solvent removed. The residue was extracted with water. The organic compound was chromatographed on a column of silica gel with ethyl acetate-hexane (9/1) as eluent. Colorless crystals were isolated when the solvent was allowed to evaporate (**Scheme 2**):

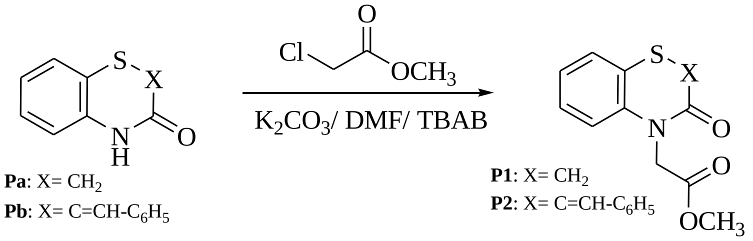

Scheme 2: Synthesis of methyl 2-(2-substituted-[1,4]-benzothiazin-3-one-4-yl) acetate (**P1 and P2**).

The analytical and spectroscopic data are conforming to the structure of compounds formed:

(P1): Yield: 72%; **MP =** 401-403 **K; NMR^{1}H (DMSO-d6) δ ppm:** 7.03-7.43 (m, 4H, H_{arom}); 4.69 (s, 2H, NCH_2); 3.67 (s, 3H, OCH_3); 3.54 (s, 2H, S-CH_2). **NMR^{13}C (DMSO-d6) δ ppm**: 169.4,166.1 (C=O); 139.7, 123.2 (Cq); 128.6, 127.8, 124.1, 118.4 (CH_{arom}); 52.6 (OCH_3); 46.8 (NCH_2); 30.6 (SCH_2).

(P2): Yield: 80%; MP = 379-381**K; NMR^{1}H (DMSO-d6) δ ppm:** 7.85 (s, 1H, =$C\underline{H}$-C_6H_5); 7.08-7.70 (m, 9H, H_{arom}); 4.85 (s, 2H, NCH_2); 3.75 (s, 3H, OCH_3). **NMR^{13}C (DMSO-d6) δ ppm:** 169.7, 162.1 (C=O); 137.0, 134.8, 120.6, 118.6 (C_q); 135.8, 131.0, 129.5, 128.5, 127.20, 124.8, 118.3 (CH_{arom}); 48.0 (NCH_2); 53.10 (OCH_3).

2.2. Preparation of solutions and specimens

The 1.0 M HCl solutions were prepared from an analytical grade 37% HCl. The concentration range of P1 and P2 inhibitors was 10^{-3} to 10^{-6} M in 1 M HCl solution. All solutions were prepared using double distilled water.

The chemical composition of the working electrode, a mild steel electrode, is given in (**Table 1**). The steel electrode was mounted in polyester. It was mechanically polished with 400, 600, 800, 1200 emery paper, washed with bi-distilled water, acetone, and then put in the cell.

Table 1. Chemical composition of steel specimens

Element	**Fe**	**C**	**Si**	**P**	**Mn**	**S**	**Al**
Mass %	99.22	0.21	0.38	0.08	0.05	0.05	0.01

The electrochemical study was carried out using a potentiostat PGZ100 piloted by Voltamaster soft-ware. This potentiostat was connected to a cell with three electrodes thermostats with double wall. A saturated calomel electrode (SCE) and platinum electrode were used as reference and auxiliary electrodes, respectively. Anodic and cathodic potentiodynamic polarization curves were plotted at a polarization scan rate of 0.5mV/s. Before doing any experiment, the potential was stabilized at free potential for 30 mins. The polarisation curves are obtained from −800 mV to −200 mV at 308 K. After that, the test solution was de-aerated by bubbling nitrogen gas. The weight loss of mild steel specimens of size 1.5× 1.5 × 0.05 cm^3 in 1 M HCl solutions without and with the different concentrations of **P1** and **P2** inhibitors was determined after immersion of 6 hrs at 308 K.

2.3. Quantum chemical calculations

Quantum chemical calculations are used to correlate experimental data for inhibitors obtained from different techniques (viz., electrochemical and weight loss) and their structural and electronic properties. According to Koop man's theorem [13], E_{HOMO} and E_{LUMO} of the inhibitor molecule are related to the ionization potential (I) and the electron affinity (A), respectively. The absolute electronegativity (χ) and global hardness (η) of the inhibitor molecule are approximated as follows[14]:

$$\chi = \frac{I+A}{2}\ ,\ \ \chi = -\frac{1}{2}(E_{HOMO} + E_{LUMO})\ \textbf{(1)}$$

$$\eta = \frac{I-A}{2}\ ,\ \ \eta = -\frac{1}{2}(E_{HOMO} - E_{LUMO})\ \textbf{(2)}$$

Where I = $-E_{HOMO}$ and A= $-E_{LUMO}$ are the ionization potential and electron affinity, respectively.

The fraction of transferred electrons ΔN was calculated according to Pearson theory [15]. This parameter evaluates the electronic flow in a reaction of two systems with different electronegativities, in particular case; a metallic surface (Fe) and an inhibitor molecule. ΔN is given as follows:

$$\Delta N = \frac{\chi_{Fe} - \chi_{inh}}{2(\eta_{Fe} + \eta_{inh})}\ \textbf{(3)}$$

Where χFe and χinh denote the absolute electronegativity of an iron atom (Fe) and the inhibitor molecule, respectively; ηFe and ηinh denote the absolute hardness of Fe atom and the inhibitor molecule, respectively. In order to apply the eq. 3 in the present study, a theoretical value for the electronegativity of bulk iron was used χFe = 7 eV and a global hardness of ηFe = 0, by assuming that for a metallic bulk I = A because they are softer than the neutral metallic atoms [15].

The electrophilicity introduced by Sastri et al [16], is a descriptor of reactivity that allows a quantitative classification of the global electrophilic nature of a compound within a relative scale. They have proposed the ω, as a measure of energy lowering owing to maximal electron flow between donor and acceptor, which defined as follows.

$$\omega = \frac{\chi^2}{2\eta}\ \textbf{(4)}$$

The Softness σ is defined as the inverse of the η [17]:

$$\sigma = \frac{1}{\eta}\ \textbf{(5)}$$

Using left and right derivatives with respect to the number of electrons, electrophilic and nucleophilic Fukui functions for a site k in a molecule can be defined[18].

$$f_k^+ = P_k(N+1) - P_k(N) \quad for\ nucleophilic\ attack\ \textbf{(6)}$$

$$f_k^- = P_k(N) - P_k(N-1) \quad for\ electrphilic\ attack\ \textbf{(7)}$$

$$f_k^+ = [P_k(N+1) - P_k(N-1)]\frac{1}{2} \quad for\ radical\ attack\textbf{(8)}$$

where, $P_k(N)$, $P_k(N+1)$ and $P_k(N-1)$ are the natural populations for the atom k in the neutral, anionic and cationic species respectively.

3. Results and Discussion

3.1. Electrochemical impedance spectroscopy measurements (EIS)

The corrosion behavior of mild steel in 1 M HCl solution at 308 K, in the absence and presence of P1 and P2, was also investigated using the electrochemical impedance spectroscopy (EIS) at 308 K. Nyquist plots of mild steel in uninhibited and inhibited acidic solutions containing various concentrations of **P1** and **P2** are shown in

(**Figures 1** and **2**). The electrochemical parameters calculated from the Nyquist plots are given in (**Table 2**). The Nyquist plots contain depressed semi-circles with their center located under the real axis, and their size increases with inhibitor concentration, indicating a charge transfer process, mainly controlling the corrosion of mild steel[19, 20]. Such a behavior is typical of solid electrodes and often referred to frequency dispersion, attributed to the surface heterogeneity due to surface roughness, impurities or dislocations [21], fractal structures, distribution of activity centers, adsorption of inhibitors, and formation of porous layers[22–25].

The diameter of the capacitive loop in the presence of inhibitor is larger than that in the absence of inhibitor, and increases with the increase of inhibitor concentration. This suggests that the impedance of inhibited substrate increases with the inhibitor concentration. Noticeably, these capacitive loops are not perfect semicircles, which can be attributed to the frequency dispersion effect as a result of the roughness and inhomogeneity of the electrode surface [26]. In the Bode plots, (**Figures 3** and **4)**, only one time constant of charge transfer and double layer capacitance were observed. These observations indicate that the corrosion of the mild steel in 1 M HCl solution is mainly controlled by a charge transfer process. The slopes of |Z| against *f* lines are not equal to -1[27]. Again, this deviation was attributed to the inhomogeneity of the mild steel surface [28]. Accordingly, the EIS data are simulated by the equivalent circuit as shown in **(Figure 7).**

Rs and R_{ct} are the solution resistance and charge transfer resistance, respectively. CPE is constant phase element to replace a double layer capacitance (C_{dl}) for more accurate fit [29]. The solid lines in (**Figures 5** and **6**) correspond to the fitted plots of the EIS experimental data using the electric circuit, which indicate that these data are fitted very well using this model.

Simulation of Nyquist and Bode plots with the above model shows excellent agreement with experimental data (**Figures 5** and **6**). This means that the suggested model could reasonably represent the charge-transfer and metal/solution interface features related to the corrosion process of mild steel in acidic solution containing **P1** and **P2** inhibitors.

The CPE is composed of a component Q_{dl} and a coefficient a, which quantifies different physical phenomena such as surface inhomogeneity resulting from surface roughness, inhibitor adsorption, and porous layer formation.

The impedance function of the CPE is represented by the following expression [30, 31]:

$$Z_{CPE} = 1/Q(jw)^n \quad \textbf{(9)}$$

Where Q is the magnitude of the CPE, *j* is the imaginary number ($j^2 = -1$), and *w* is the angular frequency. The deviation parameter ($-1 \leq n \leq +1$), has the meaning of a phase shift. For a value of n = 0, the CPE represents a pure resistor, for n = -1, it is an inductor, and for n = +1, it is a pure capacitor [32]. The double layer capacitance (C_{dl}) can be simulated via CPE from the following equation [33, 34]:

$$C_{dl} = Q_{dl} \text{ x } (2\pi f_{max})^{n-1} \quad \textbf{(10)}$$

Where f_{max} is the frequency at the maximum value of the imaginary part of the impedance spectrum.

R_{ct} value increases prominently while C_{dl} reduces with the increase of inhibitor concentration. A large charge transfer resistance (R_{ct}) is associated with a slower corroding system. At any given inhibitor concentration, R_{ct} (**P1**) <R_{ct} (**P2**), which indicates that **P2** is more efficient as corrosion inhibitor than **P1**.

The decrease in C_{dl} in the presence of inhibitor **P1** or **P2** in 1 M HCl solution, may be attributed to the decrease in local dielectric constant and/or an increase in the thickness of the electrical double layer. This means that the inhibitor molecules are adsorbed at the metal/solution interface [35].

The inhibition efficiency E_{Rct}(%) can be calculated from R_{ct} using the following equation:

$$E_{Rct}\% = \frac{R_{ct\,(inh)} - R_{ct\,(0)}}{R_{ct\,(inh)}} \text{ x } 100 \quad \textbf{(11)}$$

Where $R_{ct(0)}$ and $R_{ct(inh)}$ are the charge transfer resistance values in the absence and presence of inhibitor, respectively.

E_{Rct}(%) increases with the increase in the inhibitor concentration. The comparative study of the inhibitory potency for the tested inhibitors (**P1** and P2) shows that the inhibition efficiency of P2 is higher than of P1 at 10^{-3}M and 308 K.

Table 2. EIS parameters for the corrosion of M steel in 1 M HCl at different concentrations of **P1** and **P2** at 308K

Inhibitor	**Concentration** (M)	**R$_{ct}$** (Ω .cm^2)	**Rs** (Ω.cm^2)	**CPE** (μΩ^{-1}S^n cm-^{2})	**n**	***f*$_{max}$** (Hz)	**C$_{dl}$** (μF)	**E$_{Rct}$** (%)
1M HCl	--	14.50	1.93	393	0.88		200	--
P1	**10^{-6}**	56	3.58	313	0.78	29	99	74
	10^{-5}	81	3.60	289	0.77	20	97	82
	10^{-4}	136	3.66	135	0.79	26	45	89
	10^{-3}	340	3.11	83	0.81	15	30	**95**
P2	**10^{-6}**	75	4.20	268	0.78	23	92	81
	10^{-5}	85	6.52	287	0.77	23	83	83
	10^{-4}	213	2.93	158	0.82	10	72	93
	10^{-3}	345	3.53	116	0.81	8	58	**96**

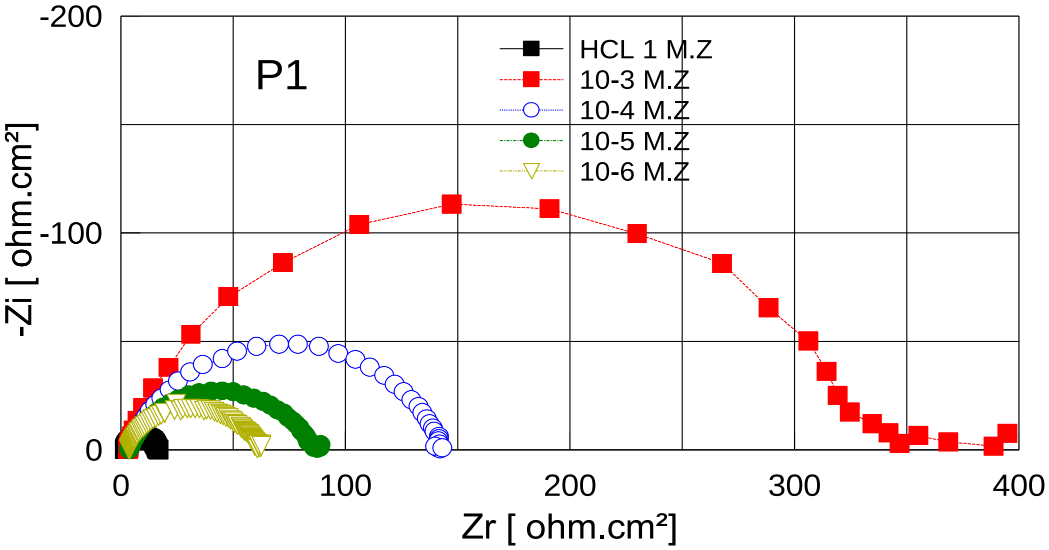

Figure 1: Nyquist diagram for mild steel in 1 M HCl at different concentrations of **P1**.

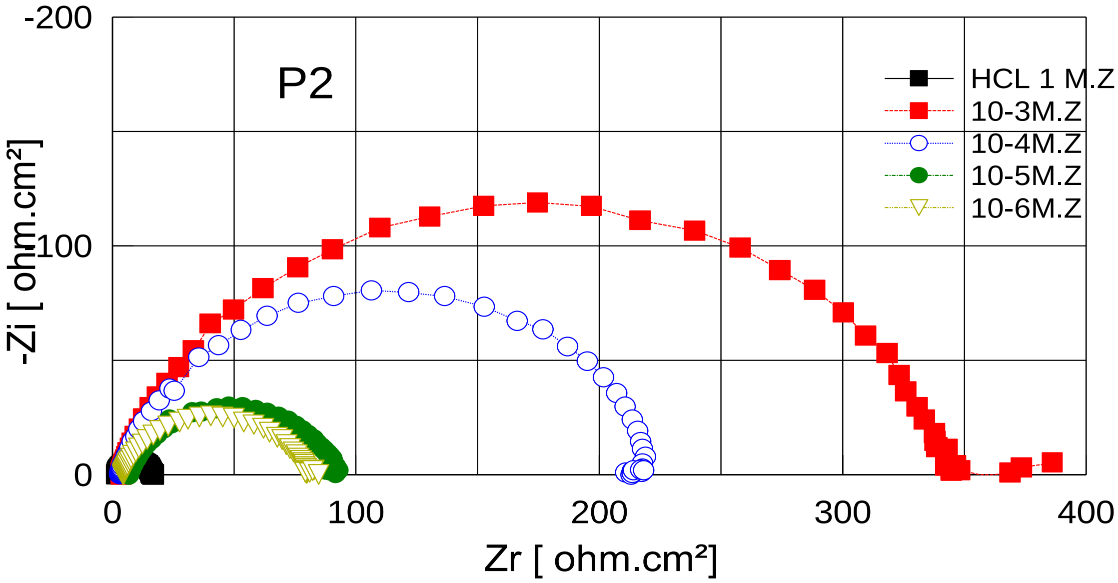

Figure 2: Nyquist diagram for mild steel in 1 M HCl at different concentrations of **P2**.

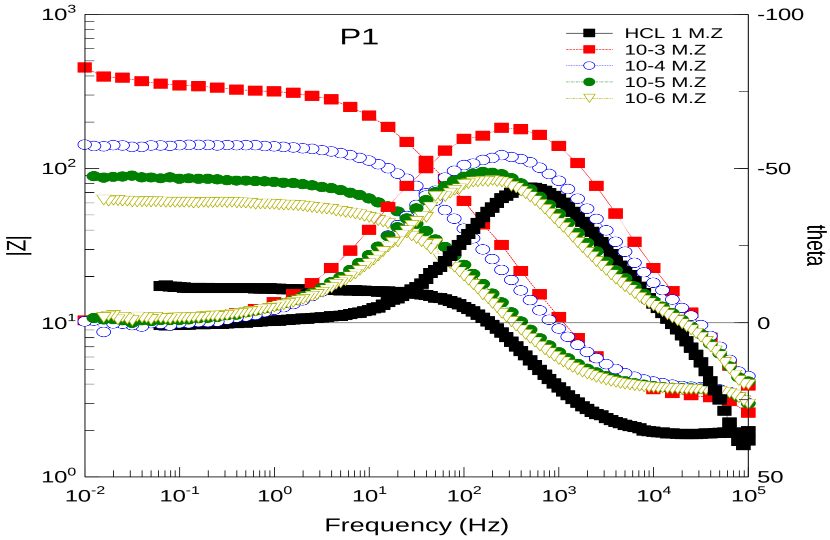

Figure 3: Bode and phase plots of mild steel in 1 M HCl at different concentrations of **P1**at 308 K.

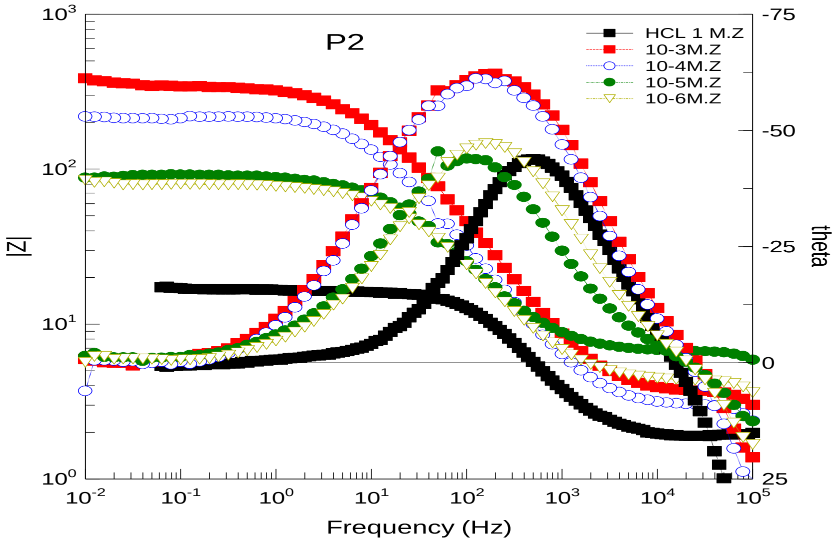

Figure 4: Bode and phase plots of mild steel in 1 M HCl at different concentrations of **P2** at 308 K.

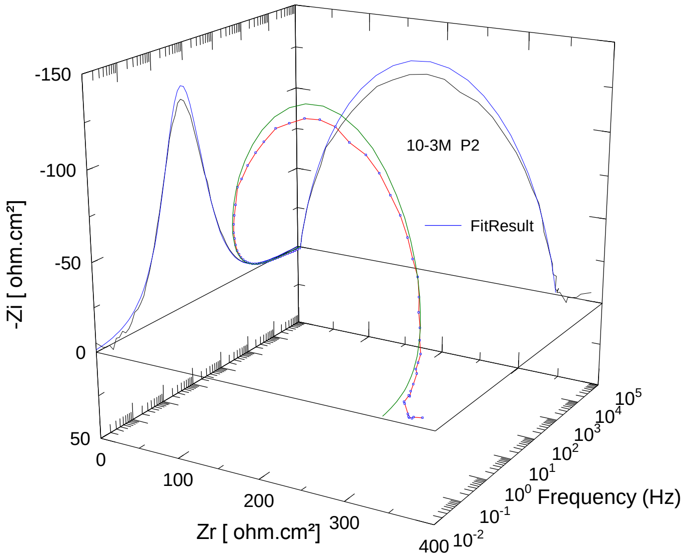

Figure 5: EIS Nyquist and Bode diagrams 3D for mild steel/1 M HCl + 10^{-3} M of **P2** interface: (------) experimental; (------) fitted data.

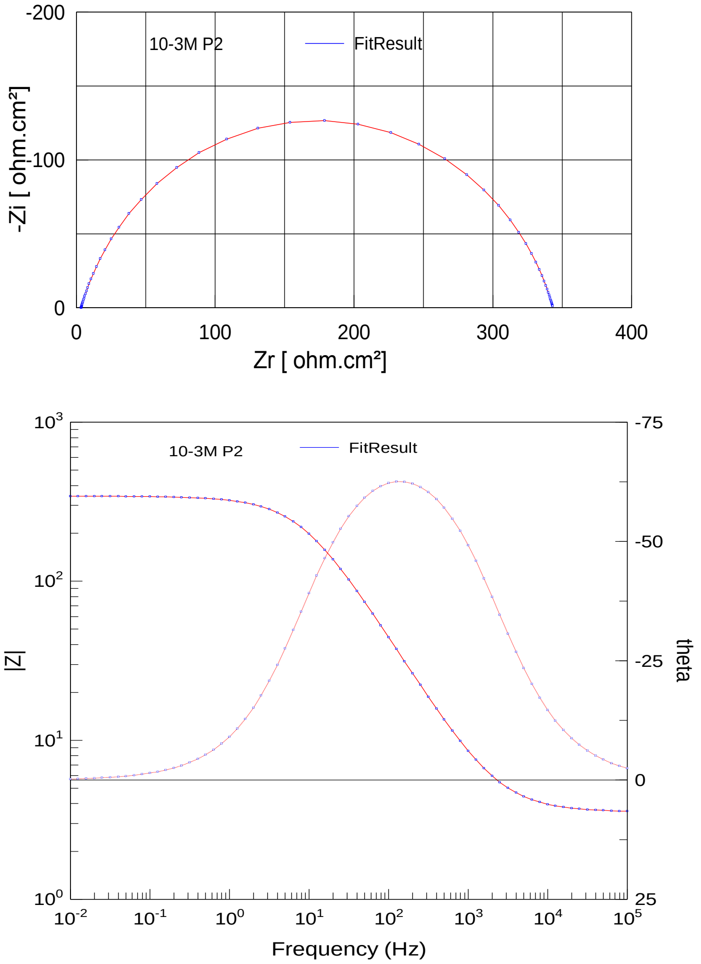

Figure 6: EIS Nyquist and Bode diagrams for mild steel/1 M HCl +10^{-3} M of **P2** interface: (red line) experimental; (blue line) fitted data using structural model in **(Figure 7)**.

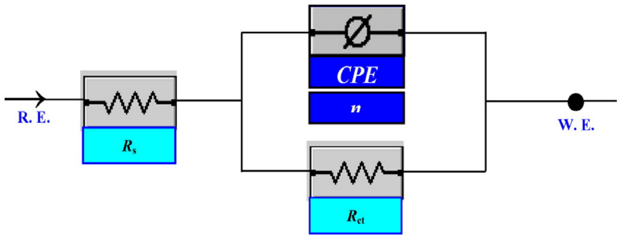

Figure 7: Equivalent circuit model used to fit the impedance spectra.

3.2. Potentiodynamic polarization curves

Potentiodynamic polarization curves of mild steel in 1 M HCl containing **P1** and **P2** at 308K are shown in (**Figures 8** and **9**), respectively. In all cases, addition of each compound causes a remarkable decrease in the corrosion rate (i.e., shifts both anodic and cathodic curves to lower current densities). In other words, both cathodic and anodic reactions of mild steel electrodes are drastically inhibited by **P1** and **P2**.

Inhibition efficiency (Ep%) is defined as:

$$Ep\% = \frac{\text{icor }(0) - \text{icor }(\text{inh})}{\text{icor }(0)} \text{x } 100 \qquad \textbf{(12)}$$

Where $i_{corr}(0)$ and $i_{corr}(inh)$ represent corrosion current density values without and with the inhibitor, respectively.

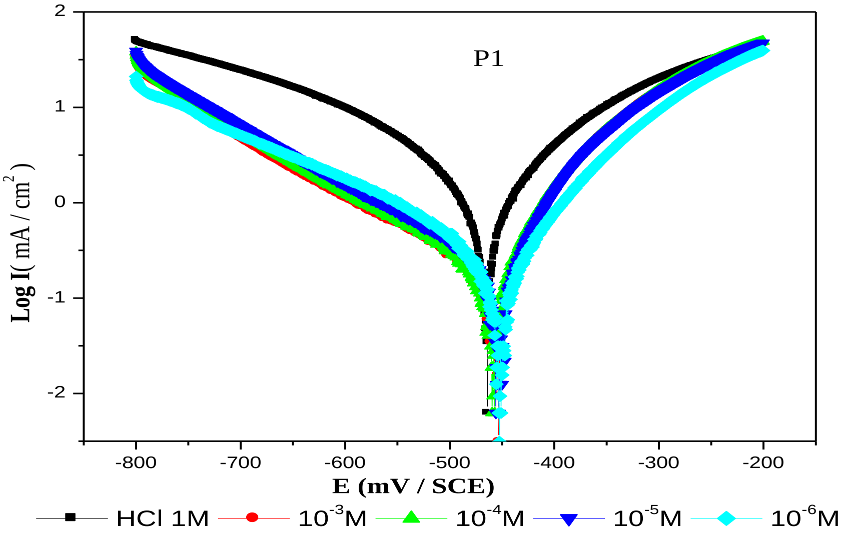

Figure 8: Potentiodynamic polarization curves for mild steel in 1 M HCl without and with different concentrations of **P1** at 308 K (immersion time = 30 mins).

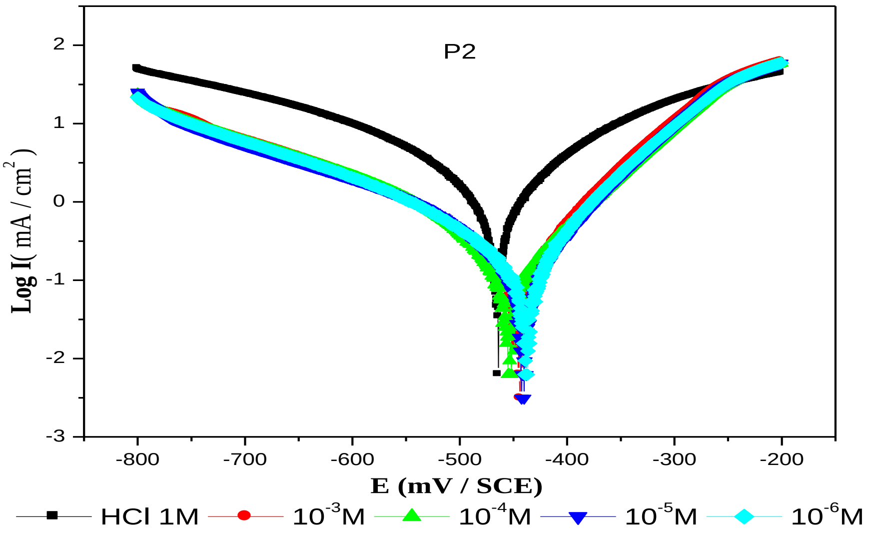

Figure 9: Potentiodynamic polarization curves for mild steel in 1 M HCl without and with different concentrations of P2 at 308 K (immersion time = 30 mins).

It should be noted that in anodic domain, it is difficult to recognize the linear Tafel regions. Accordingly, the corrosion current density values are estimated accurately by extrapolating the cathodic linear region back to the corrosion potential. Similar fitting method has also been widely used [36,37].

The electrochemical corrosion parameters including corrosion current densities (i_{corr}), corrosion potential (E_{corr}), cathodic Tafel slope (βc) and corresponding inhibition efficiency (Ep) are given in (**Table 3**). It is apparent that i_{corr} decreases considerably in the presence of each inhibitor, and decreases with increasing the inhibitor concentration. Correspondingly, Ep increases with the inhibitor concentration, due to the increase in the blocked fraction of the electrode surface by the adsorption of the inhibitor on its surface. E_p of 10^{-3} M inhibitor reaches up to a maximum of 92% for **P1** and 94% for **P2**, which again confirms that both benzothiazine derivatives **P1** and **P2** are good corrosion inhibitors for mild steel in 1 M HCl solution, and Ep for **P2** is more than **P1**, (**P2** = 94%) > **P1** = 92%).

Table 3: Potentiodynamic polarization parameters for the corrosion of mild steel in 1 M HCl solution containing different concentrations of inhibitors P1 and P2 at 308K.

Inhibitor	**Concentration (M)**	**$-E_{corr}$ (mV/SCE)**	**I_{corr} (µA/cm^2)**	**-βc (mV dec^{-1})**	**E_p (%)**
1M HCl	**-**	464	1386	184	--
P1	10^{-6}	452	419	159	70
	10^{-5}	454	256	163	82
	10^{-4}	459	168	164	88
	10^{-3}	453	107	174	**92**
P2	10^{-6}	462	391	160	72
	10^{-5}	453	225	168	84
	10^{-4}	456	128	165	91
	10^{-3}	457	81	175	**94**

The presence of **P1** or **P2** does not prominently shift the corrosion potential, which indicates that both of the studied benzothiazine derivatives (**P1** and **P2**) act as mixed-type inhibitors [38-40]. Furthermore, in the presence of each inhibitor, the slight change of βc indicates that the cathodic corrosion mechanism of mild steel does not change.

3.3. Weight loss measurements

The weight loss method for monitoring inhibition efficiency is useful because of its simple application and reliability [41,42]. In this study, the reproducibility of the results for both weight loss measurements and the inhibition efficiency was very precise (±2%) for three trials.

The inhibition efficiency (E_w%) was calculated using the following equation[43]:

$$\text{Ew}\,\% = \frac{V0-V}{V0}\ \text{X}\ 100 \quad \textbf{(13)}$$

Where $\boldsymbol{v_0}$ and $\boldsymbol{v}$ are the values of corrosion rate without and with inhibitor, respectively.

Table 4: Corrosion parameters for mild steel in 1 M HCl solution in the absence and presence of different concentrations of **P1** and **P2** obtained from weight loss measurements at 308 K.

Inhibitor	**Concentration** (M)	***v*** (mg.cm^{-2} h^{-1})	**E_w** (%)	**θ**
1M HCl	-	0.82	---	---
P1	**10^{-6}**	0.33	60	0.60
	10^{-5}	0.21	74	0.74
	10^{-4}	0.09	89	0.89
	10^{-3}	0.06	93	**0.93**
P2	**10^{-6}**	0.21	74	0.74
	10^{-5}	0.13	84	0.84
	10^{-4}	0.08	90	0.90
	10^{-3}	0.03	96	**0.96**

The inhibition efficiency (E_w%) and other parameters such as corrosion rate (*v*) and surface coverage (θ) at various concentrations of the inhibitors **P1** and **P2** are given in (**Table 4**).

Careful examination of the results showed that protection efficiencies of the studied inhibitors increase with increasing concentrations. Maximum values of (inhibition efficiency) 93% for **P1**, and 96% for **P2** were obtained at 10^{-3} M. The corrosion inhibition gets more as the inhibitor concentration becomes higher. This behavior is due to the fact that the adsorption coverage of inhibitor on mild steel surface increases with the increase in inhibitor concentration [44]. It is clearly noticed from (**Table 4**) that the inhibition efficiency of **P2** is more than **P1**. The higher inhibition efficiency of **P2** compared to **P1** is due to the presence of additional benzyl group (CHC_6H_5). The results in this study revealed that the presence of (CHC_6H_5) increases the inhibition performance. This can be attributed to the fact that the electron-rich (π electrons) of the benzyl group (CHC_6H_5) makes it very well adsorbed on the metal surface as well as the benzothiazine ring resulting in more surface coverage values (θ).

3.4. Adsorption isotherms

The most preferable way to study quantitatively the adsorbed layer of organic inhibitor responsible for the restricted access of aggressive species from the corrosive environment to the metal surface is by adsorption isotherm.

The adsorption of the studied inhibitors molecules on mild steel surface was investigated by fitting the experimental surface coverage data (θ) into various adsorption isotherms, which include Langmuir, Temkin and Frumkin models. Langmuir adsorption isotherm gave the best fit judging from near unity values of the observed regression coefficient (R^2).

The values of the slopes, intercepts, and regression coefficient for Langmuir adsorption isotherm for the studied compounds are listed in (**Table 5**). The Langmuir adsorption isotherm plots are shown in (**Figure 10**).

Table 5 clearly reveals the best fits obtained from Langmuir isotherm. Although, the values of R^2 are near unity for the Langmuir isotherm plots, but the slopes of the lines deviate appreciably from unity.

In 1 M HCl solution, **P1** and **P2** adsorption follows the Langmuir isotherm equation:

$$\frac{C}{\theta} = \frac{1}{k} + C \quad \mathbf{(14)}$$

The surface coverage values (θ) were tested graphically for fitting a suitable adsorption isotherm. In those cases, the plots of C_{inh}/θ versus C_{inh} yield a straight line, clearly proving that the adsorption of both inhibitors **P1** and **P2** on the mild steel surface in 1 M HCl obeys the Langmuir adsorption isotherm (**Figure 10**).

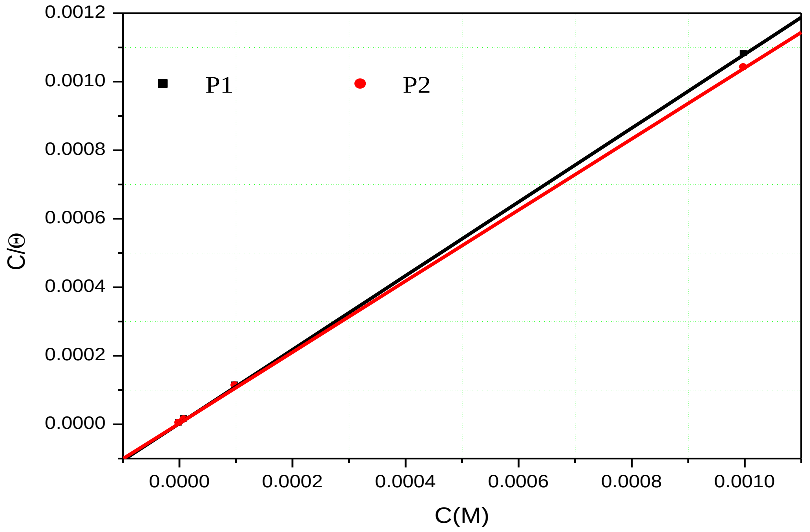

Figure 10: Langmuir adsorption isotherm for **P1** and **P2** on the mild steel surface.

The free energy of adsorption (ΔG_{ads}) at different temperature was calculated from the following equation [45, 46]:

$$\Delta G_{ads} = -RT\ln(55{,}5K) \quad \mathbf{(15)}$$

And K is given by

$$K=\theta/C_{inh}(1-\theta) \quad \mathbf{(16)}$$

Where θ is the degree of the surface coverage of the metal by the inhibitor, C_{inh} the concentration of inhibitor in mol l^{-1} and K the equilibrium constant for adsorption process.

Values of ΔG_{ads} are always used to classify adsorption process as physisorption (when ΔG_{ads} = -20 kJ mol^{-1}, or less negative) or chemisorption (for ΔG_{ads} = -40 kJ mol^{-1} or more negative). In this study, high values of K_{ads} (4.13 10^5; 3.47 10^5 M^{-1}) and large negative values of ΔG_{ads} (-43.38; -42.93 kJ mol^{-1}) suggest that the inhibitor molecules adsorbed strongly and spontaneously on the surface of mild steel.

Generally values of ΔG_{ads}until -20 kJ mol^{-1} are consistent with the electrostatic interaction between the charged molecules and the charged metal surface (physical adsorption) [47, 48]. Those about -40 kJ mol^{-1} or higher involve charge sharing or a transfer from the inhibitor molecules to the metal surface to form a coordinate type of bond (chemical adsorption) [49]. This indicates that the **P1** and **P2** taken place through electrostatic interaction between the inhibitor molecule and the mild steel surface. The large negative value of ΔG_{ads} reveals that the adsorption is chemical adsorption [50, 51].

Table 5: Thermodynamic parameters for the corrosion of mild steel in 1 M HCl solution in the absence and presence of different concentrations of **P1** and **P2**.

Inhibitor	**Linear regression coefficient** (R^2)	**Slope**	**K** (M^{-1})	ΔG_{ads} (kJ.mol^{-1})
P1	1	1.07776	4.13 10^5	-43.38
P2	0.99998	1.03754	3.47 10^5	-42.93

3.5. Computational theoretical studies

The FMOs (HOMO and LUMO) are very important for describing chemical reactivity. The HOMO containing electrons, represents the ability (E_{HOMO}) to donate an electron, whereas, LUMO haven't not electrons, as an electron acceptor represents the ability (E_{LUMO}) to obtain an electron. The energy gap between HOMO and LUMO determines the kinetic stability, chemical reactivity, optical polarizability and chemical hardness–softness of a compound [52].

In this study, the HOMO and LUMO orbital energies were calculated using B3LYP method with 6-31G which is implemented in Gaussian 09 package[53-54]. All other calculations were performed using the results with some assumptions. The higher values of E_{HOMO} indicate an increase for the electron donor and this means a better inhibitory activity with increasing adsorption of the inhibitor on the metal surface, whereas the lower values of E_{LUMO} indicates the ability to accept electron of the molecule. The adsorption ability of the inhibitor to the metal surface increases with increasing of E_{HOMO} and decreasing of E_{LUMO}. The HOMO and LUMO orbital energies of the **P1** and **P2** inhibitors were performed and were given and shown in (**Table 6**) and (**Figure 11**), respectively. High ionization energy (> 6 eV) indicates high stability of **P1** and **P2** inhibitors [55]. The number of electrons transferred (ΔN), dipole moment, ionization potential**,** electron affinity, electronegativity, hardness, softness and total energy were also calculated and tabulated in (**Table 6**).

The nucleophilicity index (ω) is higher for the **P2** inhibitor than for **P1**, which indicates that **P2** is much more rich of electrons than **P1**. The energy gap ΔE is larger for **P1** than for **P2** providing therefore a low reactivity of the **P1**.The E_{HOMO} in aqueous phase is higher in the **P2** than in the **P1**, an indication that benzyl group increases the electron donating capacity of the **P2** inhibitor.

The value of ΔN (number of electrons transferred) show that the inhibition efficiency resulting from electron donation agrees with Lukovit's study [56]. If ΔN < 3.6, the inhibition efficiency increases by increasing electron donation ability of these inhibitors to donate electrons to the metal surface [57]. The value of ΔN of **P2** (05988 and 0.5355 in gaseous and aqueous phases, receptively) is lighter than **P1** (0.5369 and 0.5052 in gaseous and aqueous phases, respectively), this indicates that **P2** is more electron donor compared to **P1**.

(**Tables 7** and **8**) display the most relevant values of the natural population (P(N), P(N-1) and P(N+1)) with the corresponding values of the Fukui functions (f_k^+, f_k^- and f_k^0) of the studied inhibitors. The calculated values of the f_k^+ for **P1** and **P2** inhibitors are mostly localized on the benzothiazine ring, namely S_{14} and O_{26} (P1) and O_{12}, S_{14} and C_{26} (P2), indicating that the benzothiazine ring may be the most probable favorite site for nucleophilic attack.

Table 6: Quantum chemical parameters for **P1** and **P2** obtained in gaseous and aqueous phases using the DFT at the B3LYP/6-31G level.

Parameter	**Gaseous Phase**		**Aqueous Phase**	
	P1	**P2**	**P1**	**P2**
Total Energy *TE* (eV)	-30045.0	-37366.5	-30045.3	-37366.9
E_{HOMO} (eV)	-6.7813	-6.4390	-6.3693	-6.7957
E_{LUMO} (eV)	-0.8549	-0.7605	-1.0609	-1.0421
Gap ΔE (eV)	5.9263	5.6785	5.9084	5.7536
Dipole moment μ (Debye)	3.3168	2.2994	4.6607	3.3799
Ionization potential I (eV)	6.7813	6.4390	6.3693	6.7957
Electron affinity A	0.8549	0.7605	1.0609	1.0421
Electronegativity χ	3.8181	3.5997	4.0151	3.9189
Hardness η	2.9632	2.8392	2.9542	2.8768
Electrophilicity index ω	2.4599	2.2820	2.7285	2.6693
Softness σ	0.3375	0.3522	0.3385	0.3476
Fractions of electron	0.5369	05988	0.5052	0.5355

Table 7: Pertinent natural populations and Fukui functions of **P1** calculated at B3LYP/6-31G in gaseous (G) and aqueous phases.

	Phase	*P(K)*	*P(K+1)*	*P(K-1)*	f^-	f^+	f^0
S14	G	15,7549	15,7910	15,4660	0,0361	0,2889	0,1625
	A	15,7358	16,4490	15,4262	0,7133	0,3096	0,5114
O26	G	8,5709	8,7485	8,5611	0,1776	0,0098	0,0937
	A	8,6106	8,6108	8,5129	0,0002	0,0976	0,0489

Table 8: Pertinent natural populations and Fukui functions of **P2** calculated at B3LYP/6-31G in gaseous (G) and aqueous phases.

	Phase	*P(K)*	*P(K+1)*	*P(K-1)*	f^-	f^+	f^0
O12	G	8,5799	8,6878	8,5590	0,1078	0,0209	0,0644
	A	8,6295	8,7203	8,6013	0,0908	0,0282	0,0595
S14	G	15,6723	15,8210	15,5011	0,1487	0,1712	0,1600
	A	15,7362	15,8231	15,3989	0,0869	0,3374	0,2121
C26	G	6,1380	6,2734	6,1213	0,1354	0,0167	0,0760
	A	6,1644	6,3220	6,0876	0,1576	0,0768	0,1172

The geometry of **P1** and **P2** in gaseous and aqueous phases (**Figure 11**) was fully optimized using DFT based on Beck's three parameters exchange functional and Lee–Yang–Parr nonlocal correlation functional (B3LYP)[58-50] and the 6–31G. The optimized molecular and selected angles, dihedral angles and bond lengths of **P1** and **P2** are given in (**Figure 11**). The optimized structure shows that the molecule P1 and have a non-planar structure. The HOMO and LUMO electrons density distributions of **P1** and **P2** are given in (**Table 9**).
The large efficiency inhibition of **P2** with respect to **P1** is due to the presence of the benzyl group in P2 inhibitor, which is electron-rich (π electrons), which increases the electron donor character of **P2.**

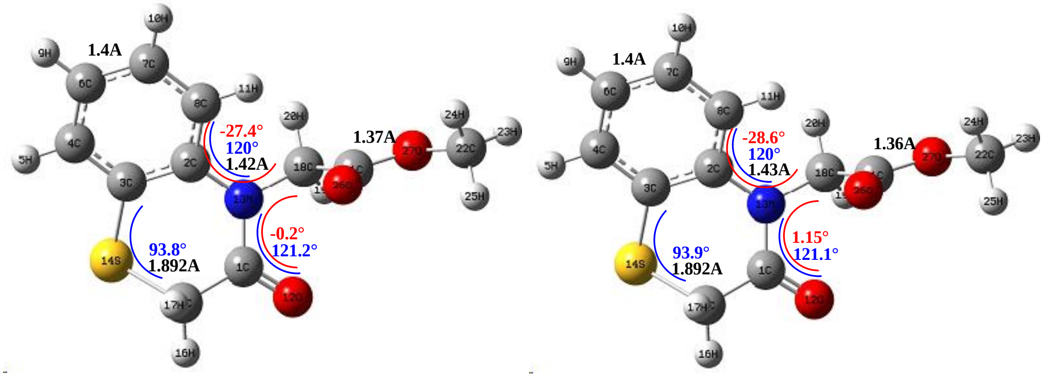

(**P1**) Gaseous phase (**P1**) Aqueous phase

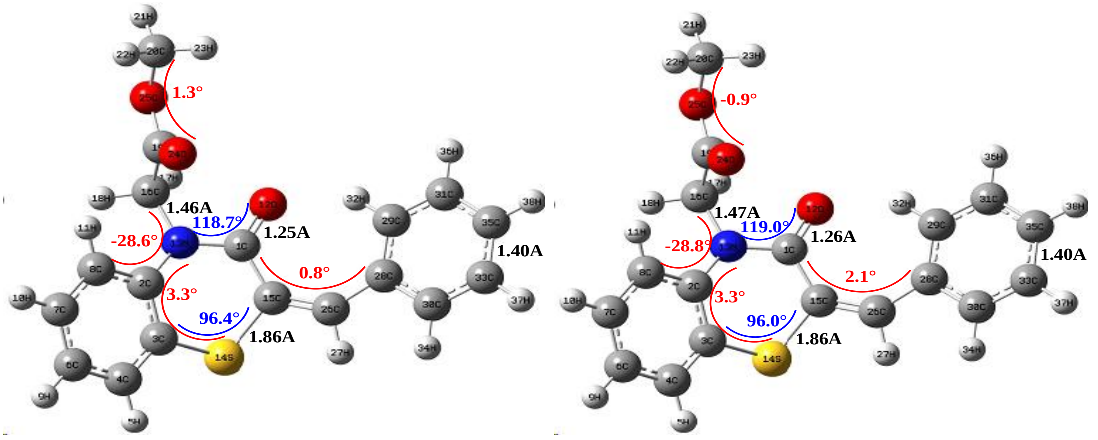

(**P2**) Gaseous phase (**P2**) Aqueous phase

Figure 11: Optimized molecular structures and selected dihedral angles (red), angles (blue) and bond lengths (black) of the studied inhibitors calculated in gaseous and aqueous phases using the DFT at the B3LYP/6-31G level

Table 9: The HOMO and the LUMO electrons density distributions of **P1** and **P2** in gaseous and aqueous phases computed at B3LYP/6-31G level for neutral forms.

Inhibitor	Type of MO	Gaseous Phase	Aqueous Phase
P1	HOMO	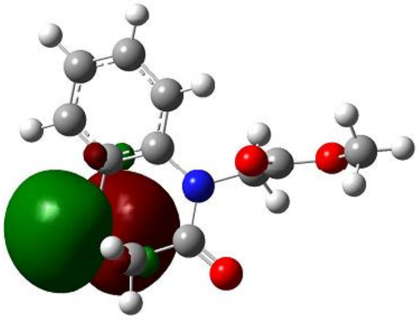	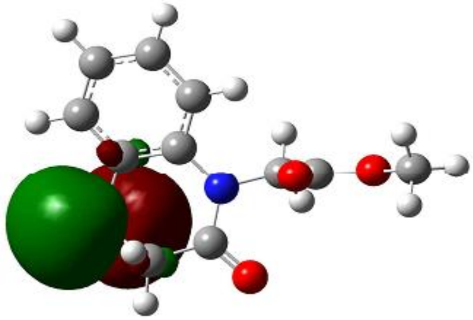
	LUMO	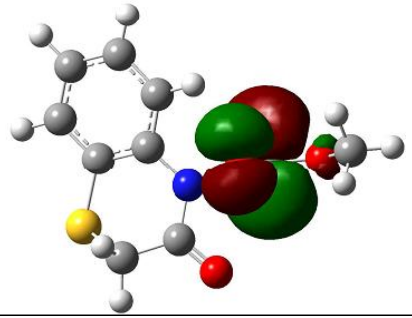	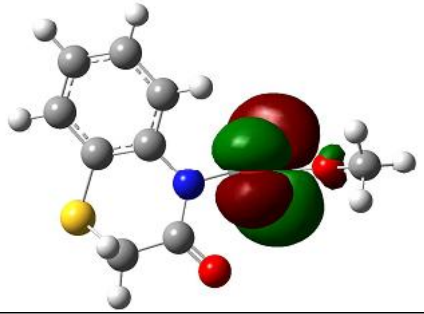

P2	HOMO	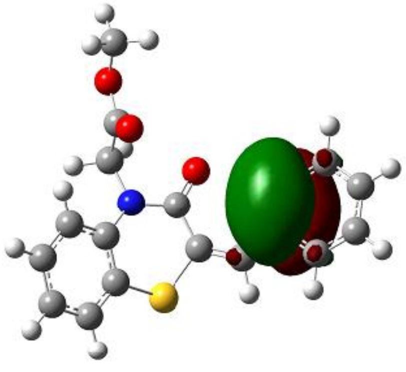	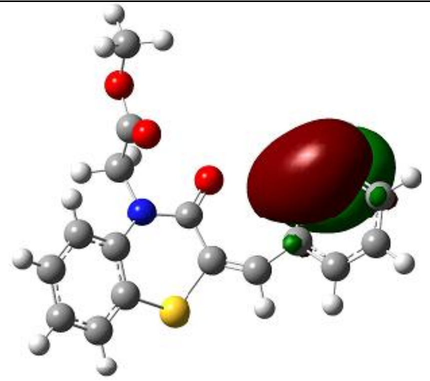
	LUMO	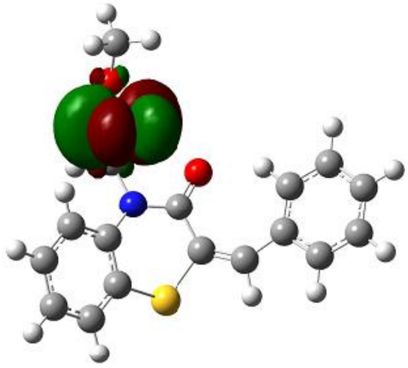	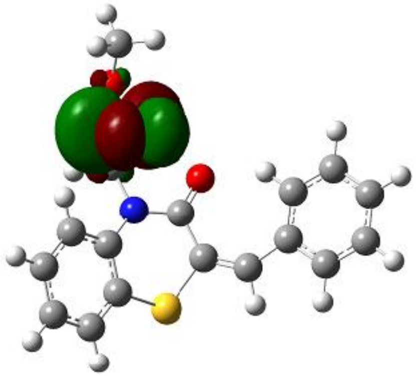

Conclusion

Corrosion inhibition characteristics of **P1** and **P2** on mild steel in 1 M HCl solution have been investigated thoroughly. The following conclusions were drawn from the results:

- **P1** and **P2** acted as efficient corrosion inhibitors for mild steel in 1 M HCl solution, and the inhibition efficiency increases with increasing their concentrations.
- The adsorption of **P1** and **P2** on mild steel obeyed the Langmuir adsorption isotherm, and this adsorption occurred via chemisorption mechanisms.
- **P1** and **P2** are mixed type inhibitors.
- Quantum chemical calculations provided more detailed accounts of how an electron donating substituent, as benzyl group (CHC_6H_5) in **P2,** tuned the extent and mode of the donor-acceptor interactions between the inhibitor molecules and metal surface and correlate the predicted adsorption energy values with experimental inhibition efficiency.

Reference

1. Bentiss F., Lagrenee M., Traisnel M., *Corrosion.* 56(2000) 733–742.
2. Pandian B. R., Qureshi A. K., Rahim A. A., Khalijah Awang H. O., *Corrosion Science.* 69(2013) 292–301.
3. Elmsellem H., Aouniti A., Toubi Y., Steli H., Elazzouzi M., Radi S., Elmahi B., El Ouadi Y., Chetouani A., Hammouti B., *Der Pharma Chemica*. 7(7)(2015) 353-364.
4. Elmsellem H., Bendaha H., Aouniti A., Chetouani A., Mimouni M., Bouyanzer A., *Mor. J. Chem.* 2(1)(2014)1-9.
5. Elmsellem H., Aouniti A., Khoutoul M., Chetouani A., Hammouti B., Benchat N., Touzani R. and Elazzouzi M., *Chem. J. Pharm. Res*. 6(4)(2014) 1216-1224.
6. Okuyama K., Kiuchi S., Okamoto M., Narita H., Kudo Y., *Eur. J. Pharmacol*. 398(2000) 209.
7. Coughlin S. A., Danz D. W., Robinson R. G., Klingbeil K. M., Wentland M. P., Corbett T. H., Waud W. R., Zwelling L.A., Altsschuler E., *Biochem E.. Pharmacol*. 50(1995)111.
8. Kawashima Y., Ota A., Mibu H., *US Patent 5496817, Chem. Abstr.* 121(1994) 108814z.
9. Sankou F., Katai H., Horiuchi Y., Kamikawa Y., *Jap Patent 2002128769, Chem. Abstr.* 136(2002) 340675n.
10. Mason J., Morize I., Menard P., Cheney D., Hulme C., Labaudiniere R., *J. Med. Chem.* 42(1999) 3251.

11. Zerzouf A., El Meslouhi H., Salem M., Essassi E. M., Pierrot M., *Acta Cryst*. E57 (2001)o362-o363.
12. Barryala Y., Massip S.P., Lazar S., Essassid E. M., Zouihri H., *Acta Cryst*. E67 (2011) o724.
13. Pearson R.G., *Inorg. Chem*. 27 (1988) 734–740.
14. Sastri V.S., Perumareddi J.R., *Corrosion*. 53 (1997) 617–622.
15. Elmsellem H., Nacer H., Halaimia F., Aouniti A., Lakehal I., Chetouani A., Al-Deyab S. S., Warad I., Touzani R., Hammouti B., *Int. J. Electrochem. Sci*. 9(2014)5328.
16. Elmsellem H., Basbas N., Chetouani A., Aouniti A., Radi S., Messali M., Hammouti B., *Portugaliae. Electrochimica. Acta*. 2(2014)77.
17. Udhayakala P., Rajendiran T. V., Gunasekaran S., *Chem.J.Biol. Phys. SCI.A.* 2(3) (2012)1151-1165.
18. Roy R.K., Pal S., Hirao K., *J. Chem. Phys*. 110(1999)8236.
19. Yadav M., Sharma U., Yadav P.N., *J. Egypt. Petrol*. 22 (2013) 335.
20. Boumhara K., Tabyaoui M., Jama C., Bentiss F., *J. Ind. Eng. Chem*. 29(2015) 146.
21. Sikine M., Kandri Rodi Y., Elmsellem H., Krim O., Steli H., Ouzidan Y., Kandri Rodi A., Ouazzani Chahdi F., Sebbar N. K., Essassi E. M., *J. Mater. Environ.Sci*. 7 (4)(2016)1386-1395.
22. Zhang F., Tang Y., Cao Z., Jing W., Wu Z., Chen Y., *Corros. Sci*. 1 (2012) 61.
23. El-Mahdy G.A., Atta A.M., Al-Lohedan H.A., Tawfik A.M., Abdel-Khalek A.A., *Int. J. Electrochem. Sci*. 10 (2015) 151.
24. Aouniti A., Elmsellem H., Tighadouini S., Elazzouzi M., Radi S., Chetouani A., Hammouti B., Zarrouk A., *Journal of TaibahUniversity for Science*. (2015), http://dx.doi.org/10.1016/j.jtusci.2015.11.008.
25. Bentiss F., Outirite M., Traisnel M., Vezin H., Lagrenee M., Hammouti B., Al-deyab S.S., Jama C., *Int. J. Electrochem. Sci*. 7, 1699 (2012).
26. Faustin M., Maciuk A., Salvin P., Roos C., Lebrini M., *Corros. Sci*. 92 (2015) 287.
27. Essaghouani A. L., Elmsellem H., Boulhaoua M., Ellouz M., El Hafi M., Sebbar N. K., Essassi E. M., Bouabdellaoui M., Aouniti A. and Hammouti B., *Der Pharma Chemica*. 8(2)(2016)347-355.
28. Elmsellem H., Nacer H., Halaimia F., Aouniti A., Lakehal I., Chetouani A., Al-Deyab S. S., Warad I., Touzani R., Hammouti B, *Int. J. Electrochem, Sci*. 9 (2014) 5328.
29. Lebrini M., Robert F., Roos C., *Int. J. Corros*. (2013) ID 139798. doi:10.1155/2013/139798.
30. Mallaiya K., Subramaniam R., Srikandan S.S., Gowri S., Rajasekaran N., Selvaraj A., *Corrosion* 64 (2008) 541.
31. Xu B., Yang W., Liu Y., Yin X., Gong W., Chen Y., *Electrochim. Acta*. 56 (2011) 3857.
32. Elmsellem H., Basbas N., Chetouani A., Aouniti A., Radi S., Messali M., Hammouti B., Portugaliae. *Electrochimica Acta.* 2 (2014) 77.
33. Elmsellem H., Karrouchi K., Aouniti A., Hammouti B., Radi S., Taoufik J., Ansar M., Dahmani M., Steli H. and El Mahi B., *Der.Pharma.Chemica*. 7(10)(2015)237-245.
34. Kosari A., Moayed M.H., Davoodi A., Parvizi R., Momeni M., Eshghi H., Moradi H., *Corros. Sci*. 78 (2014) 138.
35. Ansari K.R., Quraishi M.A., Singh A., *Corros. Sci*. 5 (2014) 79.
36. Yurt A., Ulutas S., Dal H., *Appl. Surf. Sci*. 253 (2006) 919–925.
37. Okafor P.C., Zheng Y.G., *Corros. Sci*. 51 (2009) 850–859.
38. Lahmidi S., Elmsellem H., Elyoussfi A., Sebbar N. K., Essassi E.M., Ouzidan Y., Kandri Rodi Y., Dguigui K., El Mahi B. and Hammouti B., *Der. Pharma. Chemica*. 8(1)(2016) 294.
39. Cao C., *Corros. Sci*. 38 (1996) 2073–2082.
40. A. L. Essaghouani, H. Elmsellem, M. Ellouz, M. El Hafi, M. Boulhaoua, N. K. Sebbar, E. M. Essassi, M. Bouabdellaoui, A. Aouniti., B. Hammouti, *Der. Pharma. Chemica*. 8(2)(2016)297-305.
41. N. K. Sebbar, H. Elmsellem, M. Ellouz, S. Lahmidi, E. M. Essassi, I. Fichtali, M. Ramdani, A. Aouniti, A. Brahimi., B. Hammouti, *Der. Pharma .Chemica*. 7(9) (2015) 33-42.
42. Sebbar N. K., Elmsellem H., Boudalia M., lahmidi S., Belleaouchou A., Guenbour A., Essassi E. M., Steli H., Aouniti A., *J. Mater. Environ. Sci*. 6 (11)(2015)3034-3044.

43. Elmsellem H., Youssouf M. H., Aouniti A., Ben Hadd T., Chetouani A., Hammouti B., Russian, Journal of Applied Chemistry. 87(6) (2014)744-753.
44. El Ouadi, Y., Lahhit, N., Bouyanzer, A. Elmsellem, H., Majidi, L., Znini, M., Abdel Rahman, I., Hammouti, B., El Mahi, B. and Costa, *J. International Journal of Development Research*. 6 (2016) 6867-6874.
45 Hjouji M. Y., Djedid M., Elmsellem H., KandriRodi Y., Ouzidan Y., OuazzaniChahdi F., Sebbar N. K., Essassi E. M., Abdel-Rahman I., Hammouti B.,*J. Mater. Environ. Sci*. 7 (4) (2016) 1425-1435.
46. I. Chakib, H. Elmsellem, N. K. Sebbar, E. M. Essassi, I. Fichtali, A. Zerzouf, Y. Ouzidan, A. Aouniti, B. El Mahi and B. Hammouti, *Der. Pharma. Chemica*. 8(2) (2016) 380-391.
47. Elmsellem H., Aouniti A., Youssoufi M.H., Bendaha H., Ben hadda T., Chetouani A., Warad I., Hammouti B., *Phys. Chem. News*. 70 (2013) 84.
48. Elmsellem H., Elyoussfi A., Steli H., Sebbar N. K., Essassi E. M., Dahmani M., El Ouadi Y., Aouniti A., El Mahi B., Hammouti B., *Der. Pharma. Chemica*. 8(1) (2016) 248.
49. O.K. Abiola, N.C. Oforka, *Mater. Chem. Phys*. 83 (2004) 315–322.
50. Elmsellem H., Elyoussfi A., Sebbar N. K., Dafali A., Cherrak K., Steli H., Essassi E. M., Aouniti A. and Hammouti B., *Maghr. J. Pure & Appl. Sci*. 1 (2015) 1-10.
51. Elmsellem H., Aouniti A.,Khoutoul M., Chetouani A., Hammouti B., Benchat N., Touzani R., Elazzouzi M., *J. Chem. Pharm. Res*. 6 (2014) 1216.
52. Govindarajan M., Karabacak M., *Spectrochim.Acta Part A Mol Biomol.Spectrosc*. 85 (2012) 251-60.
53. Becke A.D., *J. Chem. Phys*. 98 (1993) 1372.
54. Filali Baba Y., Elmsellem H., Kandri Rodi Y., Steli H., AD C., Ouzidan Y., Ouazzani Chahdi F., Sebbar N. K., Essassi E. M., Hammouti B., *Der Pharma.Chemica*. 8(4) (2016) 159-169.
55. Elmsellem H., Karrouchi K., Aouniti A., Hammouti B., Radi S., Taoufik J., Ansar M., Dahmani M., Steli H. and El Mahi B., *Der. Pharma. Chemica*. 7(10) (2015) 237-245.
56. Lukovits I., Kalman E., Zucchi F., *Corrosion*. 57 (2001) 3-7.
57. Sikine M., KandriRodi Y., Elmsellem H., Krim O., Steli H., Ouzidan Y., Kandri Rodi A., Ouazzani Chahdi F., Sebbar N. K., Essassi E. M., *J. Mater. Environ. Sci*. 7 (4) (2016) 1386-1395.
58. Elmsellem H., Elyoussfi A., Steli H., Sebbar N. K., Essassi E. M., Dahmani M., El Ouadi Y., Aouniti A., El Mahi B., Hammouti B., *Der. Pharma. Chemica*. 8(1) (2016) 248-256.
59. Lee C., Yang W., Parr R.G., *Phys. Rev. B.* 37 (1988) 785.
60. Chakib I., Elmsellem H., Sebbar N. K., Lahmidi S., Nadeem A., Essassi E. M., Ouzidan Y., Abdel-Rahman I., Bentiss F., B. Hammouti., *J. Mater. Environ. Sci*. 7 (6) (2016) 1866-1881.

(2016); http://www.jmaterenvironsci.com